Measurement of ^{4}He$(\vec{p},n)$ at 100 and 200 MeV: Analysis with recoil-corrected continuum shell model

C. M. Riedel,* D. Dehnhard, M. Palarczyk,† M. A. Espy,‡ M. A. Franey, and J. L. Langenbrunner‡
School of Physics and Astronomy, University of Minnesota, Minneapolis, Minnesota 55455, USA

L. C. Bland§ and D. S. Carman‖
Department of Physics, Indiana University, Bloomington, Indiana 47405, USA

B. Brinkmöller¶
Physikalisches Institut der Universität Karlsruhe, Karlsruhe, Germany

R. Madey, Y. Wang,** and J. W. Watson
Department of Physics, Kent State University, Kent, Ohio 44242, USA
(Received 26 November 2003; published 27 February 2004)

Double-differential cross sections $d^2\sigma/(d\Omega dE_x)$ and spectra of analyzing powers, A_y, for the ^{4}He$(\vec{p},n)$ reaction were measured at $T_p \approx 100$ and 200 MeV at forward angles between $\theta_{lab}=0°$ and 44°, and were analyzed using wave functions from the recoil-corrected continuum shell model (RCCSM). The steep rise of the cross-section spectra just above the $p+^3$He rest energy threshold results from the excitation of the 2^- and 1^- resonances in ^{4}Li and is well reproduced by the RCCSM at both incident energies. At higher excitation energies, the predicted cross sections fall off faster than the experimental values at forward angles. The absolute cross sections from the RCCSM were renormalized by factors of 1.3 and 1.6 at 100 MeV and 200 MeV, respectively, in order to fit the cross section summed over the lowest 10 MeV of excitation at the peak of the angular distribution. The 100 MeV A_y, averaged over the lowest 10 MeV of excitation, are well reproduced by the RCCSM but not the 200 MeV A_y, nor are the details of the A_y spectra well described at either energy.

DOI: 10.1103/PhysRevC.69.024616 PACS number(s): 25.10.+s, 25.40.Kv, 21.60.Cs, 24.70.+s

I. INTRODUCTION

This paper presents all the data taken for the ^{4}He$(\vec{p},n)$ reaction at the Indiana University Cyclotron Facility (IUCF) at two incident energies $T_p \approx 100$ MeV and 200 MeV. Subsets of the data were published previously Refs. [1,2], and presented at a conference [3]. See also Ref. [4]. Reference [1] emphasized the implications of the ^{4}He$(\vec{p},n)$ data for the mass-four system and astrophysical applications, and Ref. [2] concentrated on a comparison of the spectra from ^{3}He and ^{4}He taken at 200 MeV and their interpretation in terms of a quasifree scattering model [5–7]. This paper includes the analysis of the entire ^{4}He$(\vec{p},n)$ data set with the recoil-corrected continuum shell model (RCCSM) [8–10]. Some of this analysis was shown in Ref. [1].

The RCCSM wave functions provide a more realistic approximation to the ^{4}Li states than does the quasifree scattering formalism [5–7] employed in Ref. [2]. In the quasifree analysis, the ^{4}Li* states are obtained as potential resonances in the optical potential of the $p+^3$He channel of the $n+p+^3$He three-body final state. In the RCCSM, the unbound ^{4}Li states exist in a shell model potential well derived from the M3Y g-matrix description [11] of the nucleon-nucleon (NN) interaction.

The motivation for taking ^{4}He(p,n) data at two energies 100 and 200 MeV is the strong incident-energy dependence of the ratio of the spin-dependent isovector $(\sigma\tau)$ to the spin-independent isovector (τ) parts of the NN t matrix [12,13]. The square of the ratio of $t_{\sigma\tau}$ and t_τ at zero-momentum transfer q increases by a factor of 3 between 100 MeV and 200 MeV. Qualitatively similar comparisons persist for $q \lesssim 1.5$ fm^{-1} (e.g., Fig. 4 in Ref. [12]). The data reported in this paper span $0.2 \leqslant q \leqslant 2.3$ fm^{-1} in momentum transfer to the mass-four target. Thus, the sensitivity of the isovector (p,n) reaction, especially near threshold, to the spin-transfer $(\Delta S=1)$ versus non-spin-transfer $(\Delta S=0)$ modes of excitation is expected to be much stronger at 200 MeV than at 100 MeV.

The continuum of states in the residual ^{4}Li nucleus consists of a superposition of resonances of different multipolarities [14], each of which is expected to proceed from the

*Present address: Department of Physics, Montana State University, Bozeman, Montana 59717. Electronic address: riedel@physics.montana.edu
†Present address: Henryk Niewodniczański Institute of Nuclear Physics, 31-342 Kraków, Poland.
‡Present address: Los Alamos National Laboratory, Los Alamos, New Mexico 87545.
§Present address: Brookhaven National Laboratory, Upton, New York 11973.
‖Present address: Department of Physics and Astronomy, Ohio University, Athens, Ohio 45701.
¶Present address: S.A.P.-A.G., Walldorf, Germany.
**Present address: St. Francis Hospital, Topeka, Kansas 66606.

^{4}He(p,n) reaction either with $\Delta S=0$ or with $\Delta S=1$. Specifically, the transitions to the $J^\pi=2^-$ ground state (g.s.) and to the 1^- first excited state of ^{4}Li should become more prominent at 200 MeV than at 100 MeV, because these states are expected to arise primarily from $\Delta S=1$ transitions. The transition to the 1^- third excited state, however, is expected to be mainly $\Delta S=0$ and therefore more weakly excited at 200 MeV than at 100 MeV. The RCCSM predicts a continuum of 1^- states that are mixtures of triplet (^3P) and singlet (^1P) states with excitation-energy-dependent mixing amplitudes. Experimental data at the two energies should provide a basis for a thorough test of the spin dependence of the model calculations.

II. EXPERIMENTAL RESULTS

The experiment [2,4] was performed using the polarized proton beam at the IUCF beam swinger and neutron time-of-flight facility [15]. Neutrons from (p,n) reactions with the target were detected in NE102 plastic scintillation detectors in two stationary detector stations, and their energy spectra were reconstructed from the measured neutron time of flight. The target was a welded stainless-steel gas cell with thin Havar windows, cooled to liquid-nitrogen temperatures (77 K) and filled with ^{4}He at pressures up to 7 atm, which provided a ^{4}He thickness of $\sim$18 mg/cm^2. The yields from the ^{4}He(p,n) reaction were obtained by subtracting evacuated-target yields from ^{4}He-filled-target yields, and the neutron detection efficiencies were calibrated using measured solid-target yields from ^{12}C(p,n) and ^{13}C(p,n) and published cross sections [16–20] for these reactions. The solid-target data also determined the neutron energy calibration. We estimate an 8% systematic uncertainty in the measured cross sections, dominated by uncertainties in neutron detector efficiency, target thickness, and contributions arising from frame-overlap events (slow neutrons from a previous beam burst that arrive at the detector at the same time as fast neutrons from the current beam burst).

The double-differential cross sections and analyzing powers for the ^{4}He$(\vec{p},n)$ reaction were measured at an incident proton kinetic energy of $T_p=99.5$ MeV at eight neutron laboratory scattering angles θ_{lab} between 0° and 40°, referred to in this paper as the 100-MeV data. Measurements were made at 200 MeV in two phases: 199.9 MeV for 0° and six angles between 24° and 44°, and 199.2 MeV for four angles between 5° and 20°. The uncertainty in incident energy is estimated to be 0.5 MeV, though evidence suggests that the energies may have been on the order of 1% lower than stated above. The mean beam polarization for spin up was 68% and for spin down it was 73%, both with an estimated systematic uncertainty of 3%. A small degradation of the beam polarization through the flight path to the target was not corrected. Minor ambiguities in polarization and in incident energy do not affect the conclusions of this paper.

The cross-section spectra (double-differential laboratory cross sections) $d^2\sigma/(d\Omega\ dE_x)$ and the spectra of the analyzing powers, A_y, at 100 MeV are shown in Fig. 1 (line histogram) and Fig. 2 (data points), respectively. The data at 200 MeV are presented in Figs. 3 and 4. The cross sections and analyzing powers are displayed in the figures as a function of the excitation energy E_x in the residual ^{4}Li system. Because the g.s. of ^{4}Li is particle unstable and decays into $p+^3$He, we chose $E_x=0$ MeV at the $p+^3$He rest energy. The cross-section spectra are shown in 1-MeV binning. The analyzing powers are shown averaged over 5 MeV, except for the three largest angles at 200 MeV where the limited-statistics data were averaged over 10 MeV.

As determined from the ^{12}C$(p,n)^{12}$N calibration data, the energy resolution in the forward-angle detector station (measuring $0° \leqslant \theta_{lab} \leqslant 20°$) is better than 0.3 MeV (full width at half maximum) at 100 MeV, and 0.6 MeV at 200 MeV. The resolution at angles $\geqslant 24°$ is roughly a factor of 2 worse due to a shorter flight path to the second detector station. The full-empty target subtraction leads to a small-angle-dependent and incident-energy-dependent residual at $E_x<0$ MeV (see Figs. 1 and 3) due to frame overlap. In the worst cases, frame overlap is estimated to contribute no more than a 5% increase in cross section at $E_x=0$ MeV, and this contribution decreases with increasing E_x.

An *R*-matrix analysis by Hale, quoted in Ref. [14], of $p+^3$He elastic scattering data at $T_p \leqslant 20$ MeV places the 2^- g.s. at 4.07 MeV (full width $\Gamma=6.03$ MeV) above the $p+^3$He rest energy. Thus, with our definition of E_x, the 2^- g.s. resonance has its centroid at $E_x=4.07$ MeV. The small-angle peak shape of the 2^- state predicted by the RCCSM (long dashed line in Figs. 1 and 3, discussed in Sec. III B) is consistent with a 4-MeV centroid and a 6-MeV width. The next three states of $J^\pi=1^-(^3P)$, 0^-, and $1^-(^1P)$, are placed [14] at $E_x=4.39, 6.15$, and 6.92 MeV, with widths $\Gamma=7.35, 9.35$, and 13.51 MeV, respectively. The RCCSM 1^- state is a mixture of ^3P and ^1P, so the calculated peak shape is not easily comparable to the *R*-matrix centroids and widths, and the RCCSM 0^- is too weakly excited to be visible with the chosen vertical scales of Figs. 1 and 3. The data cover a range of E_x from -5 MeV to 30 MeV at $T_p \approx 100$ MeV and from -10 MeV to 50 MeV at 200 MeV, and the RCCSM wave functions extend up to $E_x=30$ MeV. The data and calculations, therefore, span these odd-parity states as well as parts of the even-parity resonances of $J^\pi=0^+$, 1^+, and 2^+, predicted by the RCCSM to be relatively weakly excited for $E_x \lesssim 10$ MeV, but become more strongly excited at larger E_x.

At small E_x ($\lesssim$5 MeV), the cross-section spectra are dominated by the transitions to the broad 2^- and 1^- resonances, which cause the steep rise in the cross sections just above $E_x=0$ MeV (see Figs. 1 and 3). As discussed in Ref. [2], this result is in contrast to the spectra from the ^{3}He(p,n) reaction at 200 MeV, which are dominated by a simple quasifree knockout process because there are no known resonances in the three-proton final state.

Single-differential cross sections $d\sigma/d\Omega$ were obtained by summing $d^2\sigma/(d\Omega\ dE_x)$ over the 0–10 MeV range in excitation energy. This energy bite was chosen to include the bulk of the 2^- and 1^- strength, and to highlight the momentum transfer range over which the difference between 100 and 200 MeV incident energies is strongest. The resulting angular distributions of center of mass $d\sigma/d\Omega$ and averaged A_y for this range of excitation are shown in Fig. 5 ($T_p \approx 100$ MeV) and Fig. 6 (200 MeV) as a function of center-

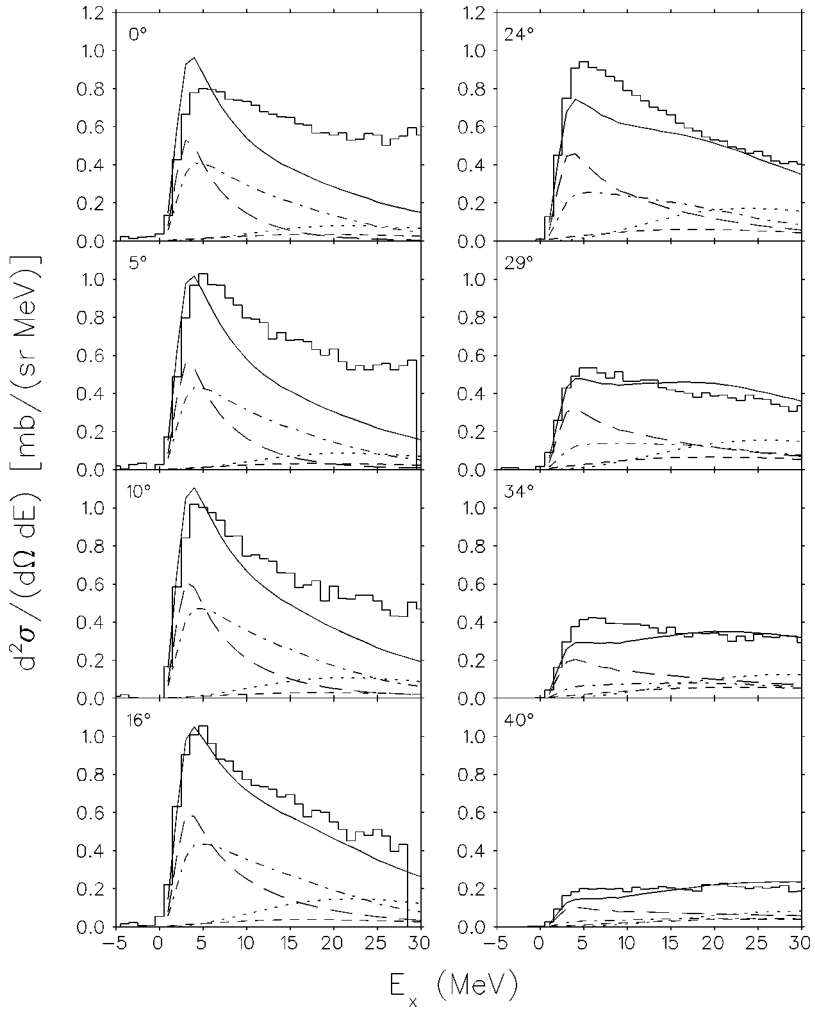

FIG. 1. ^{4}He(p,n) 100 MeV double-differential cross-section spectra (line histograms) and DWBA70 calculations using RCCSM transition amplitudes at eight angles θ_{lab}. Solid line, sum of all transitions; long dashed line, $J^\pi=2^-$; dash-dotted line, $J^\pi=1^-$; dashed line, $J^\pi=2^+$; dotted line, $J^\pi=1^+$. The calculated cross sections have been renormalized by a factor of 1.3.

of-mass angle $\theta_{\text{c.m.}}$. The 0–10 MeV excitation-energy response is clearly not dominated by $\Delta L=0$ transitions because the angular distributions do not peak at $\theta=0°$ at either 100 or 200 MeV. The A_y distributions at both energies rise sharply from zero at $\theta_{\text{c.m.}}=0°$, and then fall off slowly for larger $\theta_{\text{c.m.}}$.

III. DWIA CALCULATIONS

Calculations using the distorted wave impulse approximation (DWIA) were performed with the program DWBA70 [21]. Two sets of full direct plus exchange DWBA70 calculations were done (1) with one-particle–one-hole (1p-1h) transition densities from a simple shell model (SSM), and (2) with the transition densities calculated from the RCCSM [8–10] wave functions (Sec. III B).

The formalism on which DWBA70 is based assumes that the ^{4}He(p,n) reaction is a two-body process. DWBA70 uses harmonic oscillator wave functions to calculate the transition amplitude between the initial $p+^4$He and the final $n+^4$Li state. The ^{4}He target is parametrized as $(0s)^4$ with the oscillator parameter $b=1.2$ fm. This value reproduces the 1.676 fm root-mean-square radius of the ground state charge density of ^{4}He as measured by elastic electron scattering [22].

The initial state of the system is described as the product of a distorted wave for a proton in the presence of the $p+^4$He potential, and a bound-state wave function for a neutron in ^{4}He. The final state is the product of a distorted wave for a neutron in the presence of the $n+^4$Li potential, and a wave function for a proton assumed to be bound in ^{4}Li. The distorted waves for both the initial and final states are constructed using the optical potential of van Oers *et al.* [23] at 100 MeV, and the potential of Leung and Sherif [24] at 200 MeV. The exchange term in the potential at 100 MeV was not included due to a limitation in DWBA70, and is relatively unimportant at forward angles in the elastic scattering. The interaction that causes the transition is the free *NN t* matrix [13] acting between the proton projectile and the bound neutron.

A. DWIA with simple shell model wave functions

The SSM 1p-1h transitions can be used to investigate the sensitivity of the DWIA cross sections and analyzing powers to optical potentials, the excitation energy, different parts of the *NN* force, etc. These calculations also allow a separation of the $J^\pi=1^-(^3P)$ from the $1^-(^1P)$ so that spin-dependent and spin-independent effects can be isolated, a separation that is not possible with the RCCSM transition densities. The excitation energy at which the distorted waves were calculated

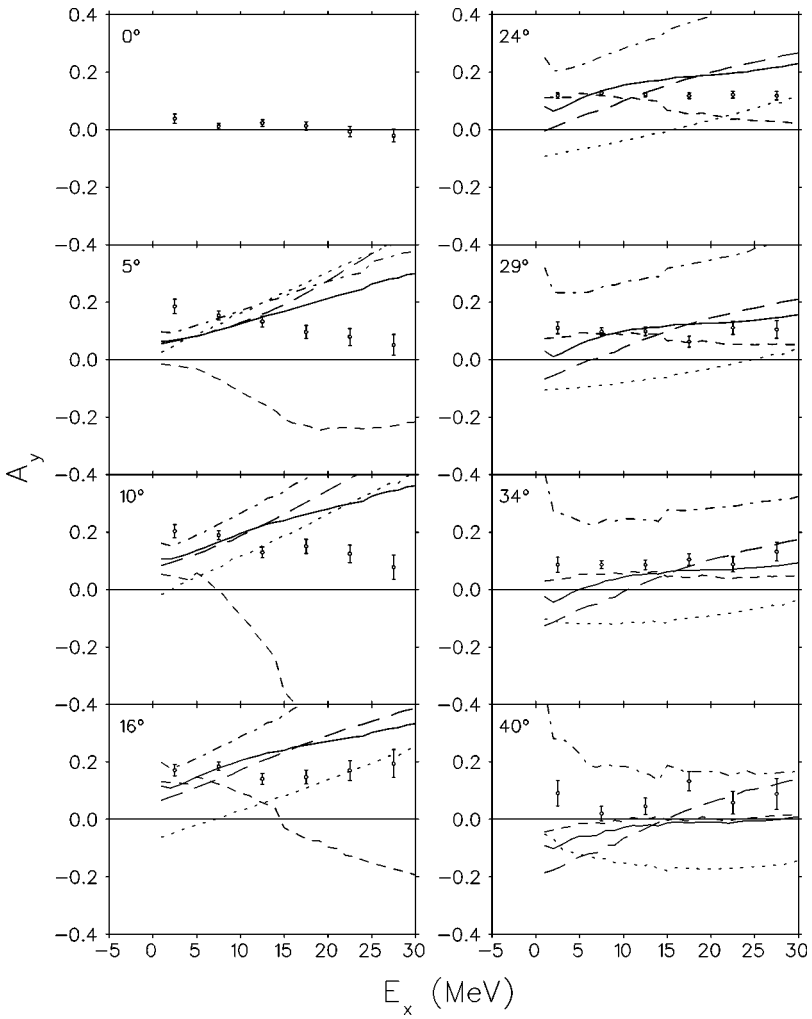

FIG. 2. ^{4}He($\vec{p},n$) 100 MeV analyzing power spectra and DWBA70 predictions using RCCSM transition amplitudes. The line types are described in Fig. 1, but with the solid line showing the cross-section averaged A_y. Frror bars include statistics only.

was 23 MeV above the g.s. of ^{4}He. This energy is near the centroid of the $J^\pi=2^-$ state in ^{4}Li. Variations in the value of the excitation energy used caused relatively small, angle-dependent effects on the calculated observables.

Summing all four negative-parity transitions $J^\pi=2^-,1^-(^3P),0^-$, and $1^-(^1P)$, the small E_x cross-section data fall off much faster as a function of angle than the calculations. The inclusion of the positive-parity transitions does not reduce the discrepancy appreciably. In order to fit the shape of the angular distribution of the data better, an unrealistically large value of $b=1.7$ fm is required. The analyzing powers, however, are remarkably well reproduced with the value of $b=1.2$ fm. This is especially surprising, and probably fortuitous, at 100 MeV, where the optical potential was fit to elastic cross sections only (i.e., no A_y).

Calculations using SSM 1p-1h wave functions give angular distributions for individual multipolarities, but not the shapes of the spectra. They also do not describe the quasifree neutron knockout process. In addition, the simple 1p-1h transition densities calculated with harmonic oscillator wave functions in DWBA70 do not have the proper recoil corrections nor do they include transitions to unbound states.

B. DWIA with recoil-corrected continuum shell model wave functions

A significant step beyond the SSM approach is the use of the wave functions from the RCCSM [8–10], which is based on the *R*-matrix approach of Lane and Robson [25], and has been very successful in describing transitions to the mass-four continuum [9]. The RCCSM properly treats the unbound nature of the states in ^{4}Li in such a way that quasifree scattering and inelastic scattering to excited states are described simultaneously and cannot be separated. The conventional continuum shell model, which uses coordinates relative to the total center-of-mass coordinate, contains errors that arise from a spurious excitation of the center-of-mass coordinate. The RCCSM corrects for this problem and accounts for some recoil effects, which are particularly important for light nuclei.

The RCCSM has been applied in the description of cross sections for inelastic scattering from ^{4}He to states in the ^{4}He continuum. In an analysis of the ^{4}He(e,e')^{4}He* reaction [26] at 180°, the RCCSM cross sections were multiplied by a center-of-mass correction factor of 1.4 at 130 MeV incident energy and 2.4 at 200 MeV. In those calculations, the con-

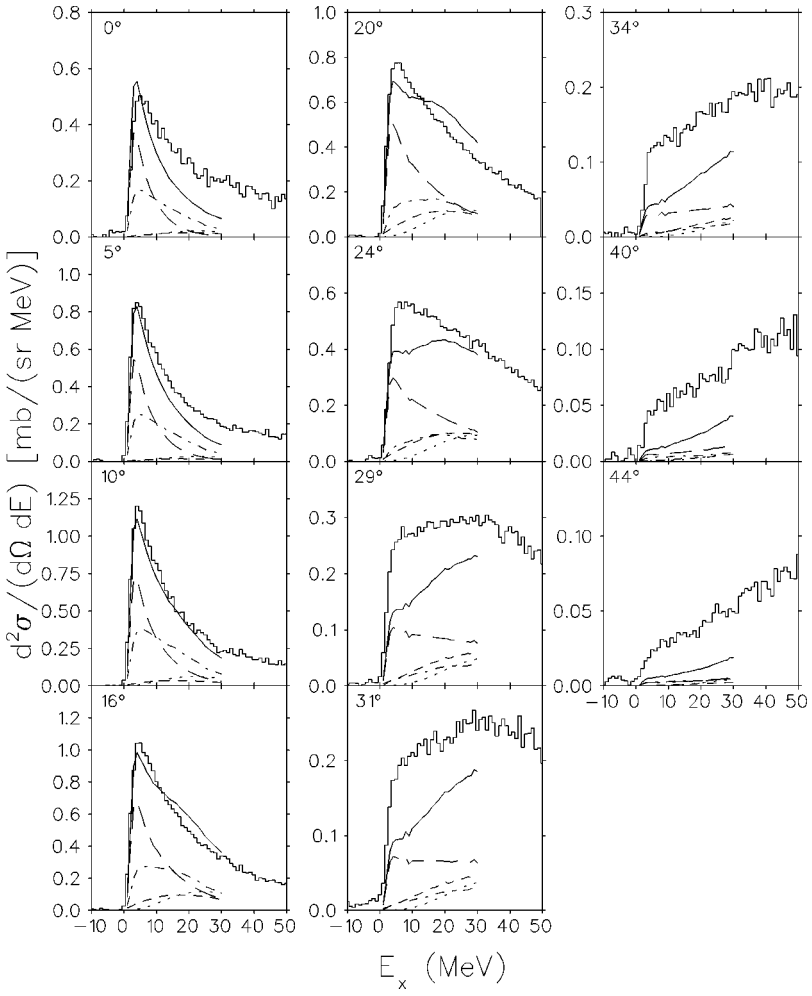

FIG. 3. ^{4}He(p,n) 200 MeV double-differential cross-section spectra and DWBA70 predictions using RCCSM transition amplitudes. The line types are described in Fig. 1. All calculations have been renormalized by a factor of 1.6.

tribution of the recoiling core to the form factors was ignored and the ground state was taken as pure $(0s)^4$. In two subsequent calculations [27,28] which include the core contributions, correlations in the ground state, and meson-exchange currents, the correction factors were not necessary, and good agreement with the data was achieved. These calculations demonstrated that the core contribution becomes more important with increasing momentum transfer. The calculations reported in this present paper also neglect the core contribution and employ a $(0s)^4$ g.s. because DWBA70 is not organized to handle all of the Jacobi coordinates. Hence, one expects to see in this ^{4}He(p,n)^{4}Li* work, in the ^{4}He(π,π')^{4}He* work of Blilie *et al.* [29], and in the ^{4}He($\vec{p},p'$)^{4}He* work of Sterbenz *et al.* [30], the same order of error, increasing with momentum transfer, as one sees in comparing the calculations of Hotta *et al.* [26] and Halderson [27,28].

In the ^{4}He(π,π')^{4}He* work [29] at 180 MeV incident energy, the RCCSM was found to describe the measured double-differential cross-section spectra fairly well after renormalizing only the cross section for the transition to the $J^\pi=2^-$ by a factor of 1.35. In the ^{4}He($\vec{p},p'$)^{4}He* work [30], cross sections were obtained at incident energies of 500 MeV and 800 MeV for 2-MeV bites of the continuum between $E_x=22$ and 34 MeV. The RCCSM predictions for the cross sections were found to be approximately a factor of 2 too small and the analyzing powers a factor of 2 too large relative to the data, but the shapes of the angular distributions and the qualitative features of the analyzing power data were described reasonably well by the RCCSM.

In this paper, we present DWIA calculations using the RCCSM wave functions for the ^{4}He($\vec{p},n$)^{4}Li* reaction, with the same optical potentials [23,24] and *NN* forces [13] as were applied in the SSM studies. The RCCSM wave functions for the unbound proton in ^{4}Li are constructed as a sum over a basis of harmonic oscillator bound-state wave functions. The RCCSM provides E_x-dependent expansion coefficients in terms of these basis states for each multipole component, and includes higher *s*, *p*, *d*, and *f* orbitals up to principal quantum number $n=8$. The oscillator parameter $b=1.2$ fm was used for all of the harmonic oscillator expansion states. The radial integration grid was scaled by a factor $A/(A-1)=4/3$ to correct for the Jacobi coordinate used in the RCCSM and the center-of-mass radial coordinate used in DWBA70. In order to expedite the calculations, the distorted waves for the $n+^4$Li channel are calculated only once at $E_x=5$ MeV and used for all excitation energies. As we found in the SSM calculations, use of the correct value of E_x marginally increases only the small-angle cross sections at large excitation energies and therefore would slightly improve the agreement with the data.

In Figs. 1–6, the DWIA results for cross sections and analyzing powers using the RCCSM wave functions in

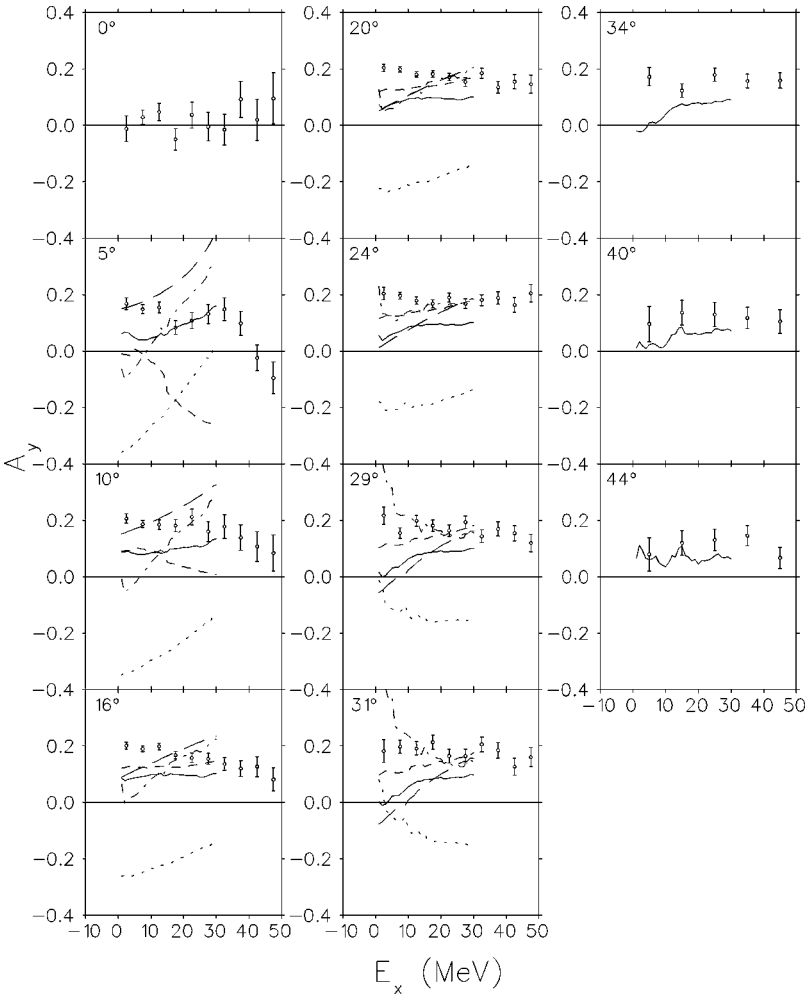

FIG. 4. ^{4}He$(\vec{p},n)$ 200 MeV analyzing power spectra and DWBA70 predictions using RCCSM transition amplitudes. The line types are described in Figs. 1 and 2. For clarity, only the averaged A_y is shown for 34°, 40°, and 44°.

DWBA70 are shown for comparison with our 100- and 200-MeV ^{4}He$(\vec{p},n)$ data. To fit the measured cross sections integrated from 0 to 10 MeV in E_x at the peak of the angular distribution, the 100-MeV calculations for all multipolarities were renormalized by a factor of 1.3, and the 200-MeV calculations were renormalized by a factor of 1.6. These renormalizations are dependent on our choice of the 0–10 MeV E_x bite, but are consistent with the magnitude of the renormalizations required in the (e,e') [26], (π,π') [29], and (p,p') [30] work.

Near the peak of the angular distribution ($\theta_{lab} \approx 10°$), the DWIA calculations reproduce the shapes of the measured cross-section spectra (Figs. 1 and 3), especially the region $E_x < 10$ MeV, which is dominated by the $L=1$ resonances. This qualitative agreement mirrors the agreement found in the (e,e') work [26] at comparable q^2. We note that the RCCSM calculates the mass-four continuum wave functions allowing only for two-body breakup, i.e., $^4\mathrm{Li}^* \rightarrow p + {}^3\mathrm{He}$. With increasing excitation energy, multiparticle breakup is expected to contribute to the measured inclusive spectra. For example, the threshold for the three-body breakup channel, $^4\mathrm{Li}^* \rightarrow d + 2p$, is at $E_x = 5.5$ MeV.

The angular dependence of the experimental center-of-mass cross sections for the energy interval between 0 and 10 MeV is also well described (upper panels of Figs. 5 and 6). At larger angles at 200 MeV, the renormalized DWIA predictions fall below the cross-section data, presumably due in part to the omission of multiple particle breakup channels, as may also be the case at higher excitation energies. Good agreement at forward angles was also found in the quasifree calculations [2] at 200 MeV and in the (p,p') work [30].

As expected, the transitions to unnatural parity states are predicted to be relatively more strongly excited at 200 MeV than at 100 MeV. For example, the transition to 2^- is exclusively a $\Delta S=1$ transition and is stronger at 200 MeV than at 100 MeV, whereas the transition to the 1^- is a mixture of $\Delta S=0$ and $\Delta S=1$ and is weaker at 200 MeV than at 100 MeV.

At both 100 and 200 MeV, the spectra of measured analyzing powers (Figs. 2 and 4) are quite flat, with a slight decreasing trend as a function of E_x near the peak of the angular distributions. The RCCSM predictions follow a slight increasing trend as a function of E_x. The angular distribution of A_y averaged over $0 < E_x < 10$ MeV at 100 MeV (Fig. 5) is fitted quite well by the RCCSM calculations considering the optical potential was not fit to elastic A_y. At 200 MeV (Fig. 6), however, the predicted A_y fall approximately a factor of 2 below the measured A_y at small angles. The 200 MeV A_y are better fit by the quasifree calculations presented in Ref. [2] (Fig. 11 and the lower panel in Fig. 12), whereas the RCCSM calculations strongly resemble the free *NN* charge exchange A_y [31] also shown in Ref. [2] (solid

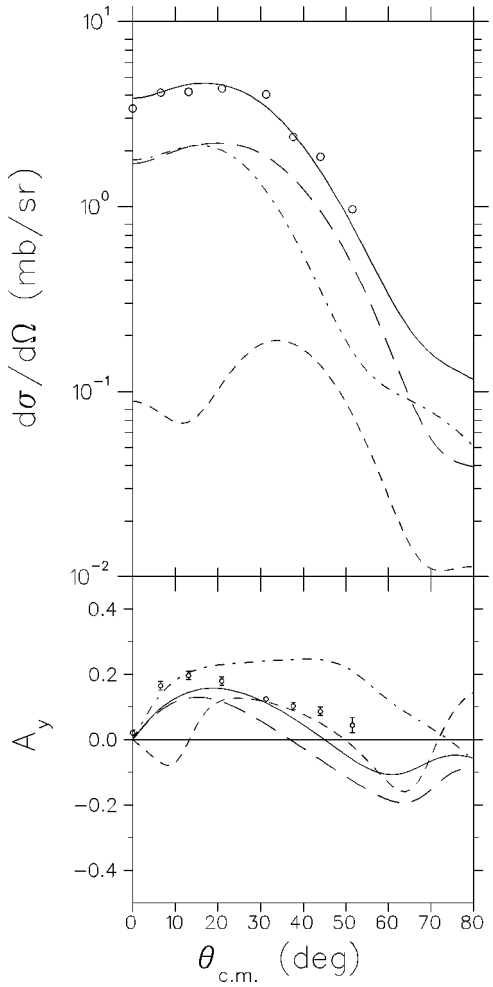

FIG. 5. ^{4}He(p,n) 100 MeV angular distributions of center-of-mass cross sections (upper panel) and analyzing powers (lower panel), and DWBA70 predictions using RCCSM transition amplitudes. The cross section data and calculations have been integrated over the 0–10 MeV range in excitation energy, and the calculated cross section has been renormalized by a factor of 1.3. Uncertainties in the cross-section data are smaller than the plotting symbol. The analyzing power data and calculations have been averaged over the 0–10 MeV range in E_x. The line types are described in Figs. 1 and 2.

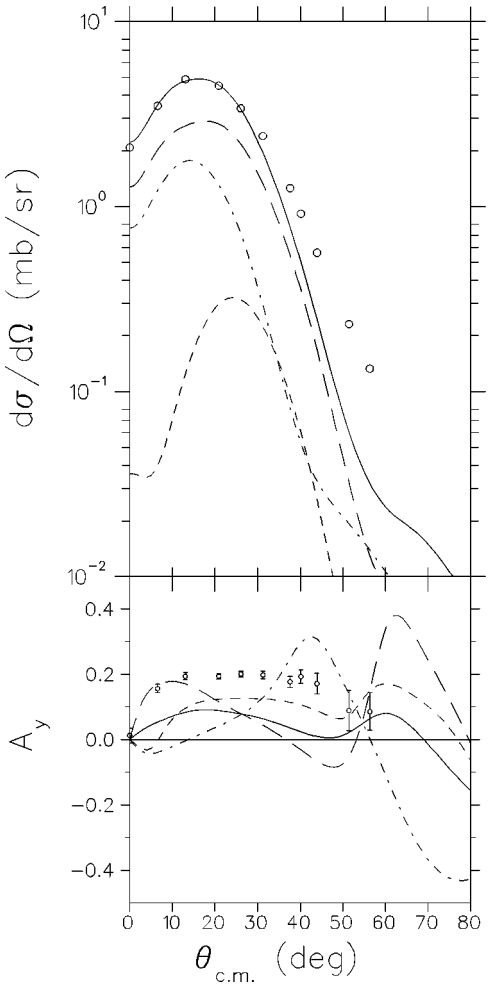

FIG. 6. ^{4}He(p,n) 200 MeV angular distributions of center-of-mass cross sections and analyzing powers with DWBA70 calculations using RCCSM transition amplitudes. The cross-section data and calculations have been integrated over the 0–10 MeV range in excitation energy, and the calculated cross section has been renormalized by a factor of 1.6. The analyzing power data and calculations have been averaged over the 0–10 MeV range in E_x. The line types are described in Figs. 1 and 2.

line in lower panel of Fig. 12). Therefore, the three-body final state, which is incorporated into the formalism of the quasifree calculations but not into the RCCSM calculations, may be especially important to the description of polarization observables.

IV. CONCLUDING REMARKS

As mentioned above, inclusion of core contributions and ground state correlations brought the higher momentum transfer (e,e') calculations into agreement with data. These effects were also included in ^{4}He($\pi,\pi' p$) calculations [32], where their inclusion was absolutely necessary to explain the anomalous values of $\sigma(\pi^+,\pi^{+\prime}p)/\sigma(\pi^-,\pi^{-\prime}p)$ [33]. An interesting theoretical work would be the inclusion of these effects for ^{4}He(p,n)^{4}Li.

ACKNOWLEDGMENTS

The authors wish to thank the staff at IUCF for technical assistance. We are especially grateful to Professor D. Halderson for providing us with the RCCSM wave functions, for numerous helpful discussions, and for a critical reading of the manuscript. This work was supported in part by the U.S. Department of Energy and the National Science Foundation.

[1] C. M. Edwards *et al.*, Phys. Lett. B **368**, 39 (1996); **380**, 493(E) (1996).
[2] M. Palarczyk *et al.*, Phys. Rev. C **58**, 645 (1998).
[3] C. M. Edwards *et al.*, in *Polarization Phenomena in Nuclear Physics*, edited by Edward J. Stephenson and Steven E. Vigdor, AIP Conf. Proc. No. 339 (AIP, Woodbury, NY, 1995), p. 438.
[4] C. M. Edwards, Ph.D. thesis, University of Minnesota, 1996; National Nuclear Data Center, Experimental Nuclear Reaction Data, Brookhaven National Laboratory, 2000 http://www.nndc.bnl.gov/nndc/exfor/.
[5] N. S. Chant and P. G. Roos, Phys. Rev. C **15**, 57 (1977).
[6] N. S. Chant, P. Kitching, P. G. Roos, and L. Antonuk, Phys. Rev. Lett. **43**, 495 (1979).
[7] N. S. Chant and P. G. Roos, Phys. Rev. C **27**, 1060 (1983).
[8] R. J. Philpott, Nucl. Phys. **A289**, 109 (1977).
[9] D. Halderson and R. J. Philpott, Nucl. Phys. **A321**, 295 (1979).
[10] D. Halderson and R. J. Philpott, Nucl. Phys. **A359**, 365 (1981).
[11] G. Bertsch, J. Borysowicz, H. McManus, and W. G. Love, Nucl. Phys. **A284**, 399 (1977).
[12] W. G. Love and M. A. Franey, Phys. Rev. C **24**, 1073 (1981).
[13] M. A. Franey and W. G. Love, Phys. Rev. C **31**, 488 (1985).
[14] R. R. Tilley, H. R. Weller, and G. M. Hale, Nucl. Phys. **A541**, 1 (1992).
[15] C. D. Goodman, C. C. Foster, M. B. Greenfield, C. A. Goulding, D. A. Lind, and J. Rapaport, IEEE Trans. Nucl. Sci. **26**, 2248 (1979).
[16] J. N. Knudson, B. D. Anderson, P. C. Tandy, J. W. Watson, R. Madey, and C. C. Foster, Phys. Rev. C **22**, 1826 (1980).
[17] G. L. Moake, L. J. Gutay, R. P. Scharenberg, P. T. Debevec, and P. A. Quin, Phys. Rev. Lett. **43**, 910 (1979).
[18] X. Yang *et al.*, Phys. Rev. C **48**, 1158 (1993).
[19] J. Rapaport, T. Taddeucci, C. Gaarde, C. D. Goodman, C. C. Foster, C. A. Goulding, D. Horen, E. Sugarbaker, T. G. Masterson, and D. Lind, Phys. Rev. C **24**, 335 (1981).
[20] T. N. Taddeucci, C. A. Goulding, T. A. Carey, R. C. Byrd, C. D. Goodman, C. Gaarde, J. Larsen, D. Horen, J. Rapaport, and E. Sugarbaker, Nucl. Phys. **A469**, 125 (1987).
[21] R. Schaeffer and J. Raynal, DWBA70 1970, computer program with modifications by M. A. Franey.
[22] H. de Vries, C. W. de Jager, and C. de Vries, At. Data Nucl. Data Tables **36**, 495 (1987).
[23] W. T. H. van Oers *et al.*, Phys. Rev. C **25**, 390 (1982).
[24] S. W.-L. Leung and H. S. Sherif, Can. J. Phys. **56**, 1116 (1978).
[25] A. M. Lane and D. Robson, Phys. Rev. **151**, 774 (1966); **178**, 1715 (1969); **185**, 1403 (1969).
[26] A. Hotta, J. Dubach, R. S. Hicks, R. L. Huffman, B. Parker, G. A. Peterson, P. J. Ryan, R. P. Singhal, and D. Halderson, Phys. Rev. C **38**, 1547 (1988).
[27] D. Halderson, Phys. Rev. C **45**, 42 (1992).
[28] D. Halderson, Phys. Rev. C **53**, 2978 (1996).
[29] C. L. Blilie *et al.*, Phys. Rev. Lett. **57**, 543 (1986).
[30] S. M. Sterbenz, D. Dehnhard, M. K. Jones, S. K. Nanda, C. E. Parman, Y.-F. Yen, K. W. Jones, and C. L. Morris, Phys. Rev. C **45**, 2578 (1992).
[31] R. A. Arndt and L. D. Roper, SAID, 1995, solution SM95, Scattering Analysis Interactive Dial-in Program, Virginia Polytechnic Institute and State University.
[32] D. Halderson and V. A. Sadovnikova, Phys. Rev. C **56**, 2688 (1997).
[33] M. K. Jones *et al.*, Phys. Rev. C **42**, R807 (1990); **46**, 52 (1992).